Activation of Topological Defects Induces a Brittle-to-Ductile Transition in Epithelial Monolayers

Yixia Chen, Qigan Gao, Jingchen Li, Fangtao Mao, Ruowen Tang, and Hongyuan Jiang*
Hefei National Laboratory for Physical Science at the Microscale, CAS Key Laboratory of Mechanical Behavior and Design of Materials, CAS Center for Excellence in Complex System Mechanics, Department of Modern Mechanics, University of Science and Technology of China, Hefei, Anhui 230026, China

(Received 7 June 2021; accepted 8 December 2021; published 5 January 2022)

Epithelial monolayers are subjected to various mechanical forces, such as stretching, shearing, and compression. Thus, its mechanical response to external loadings is essential for its biological functions. However, the mechanism of the fracture failure of the epithelial monolayer remains poorly understood. Here, by introducing a new type of topological transition, i.e., detach transition or $T4$ transition, we develop a modified cellular vertex model to investigate the rupture of the cell monolayer. Interestingly, we find a brittle-to-ductile transition in epithelial monolayers, which is controlled by the mechanical properties of single cells and cell-cell contacts. We reveal that the external loadings can activate cell rearrangement in ductile cell monolayers. The plastic deformation results from the nucleation and propagation of "pentagon-heptagon defects" in analogy with the topological defects commonly seen in 2D materials. By using a simplified four-cell model, we further demonstrate that the brittle-to-ductile transition is induced by the competition between cell rearrangement and cell detachment. Our work provides a new theoretical framework to study the rupture of living tissues and may have important implications for many other biological processes, such as wound healing and tissue morphogenesis.

DOI: 10.1103/PhysRevLett.128.018101

An epithelial monolayer, a single-cell-thick tissue that covers most surfaces of animal organs, is subjected to various internal or external mechanical forces and thus undergoes large deformations during embryonic morphogenesis [1–3] and many physiological activities such as respiration, digestion, and cardiac pulses [4–6]. For example, the typical strain of human skin during posture changes or sports is about 25% [7]. Cyclic changes in blood pressure can stretch blood vessel walls circumferentially and induce a strain up to 15% [8]. The maximum strain and strain rate of mitral valve during the beating of human hearts can reach 30% and 400% s^{-1}, respectively [9,10]. Furthermore, the compressive forces during embryonic development are big enough to buckle and fold tissues [11] and drive the morphogenesis of brain cortex [12], gut villi [13], and optic cup [14]. Thus, the mechanical properties of epithelial monolayers must be excellent enough to maintain their integrity under these mechanical loadings.

Despite the fact that epithelial monolayers can dissipate mechanical stress to maintain epithelial homeostasis through cell division, intercalation, and extrusion [15–19], tissue fracture may still occur when cell-cell adhesion is impaired or excessive stretch is applied. For example, patients with mutations in adherens junction proteins, desmosomal proteins, or actin regulators suffer from tissue fragility defects and disrupted barrier functions [20]. Mechanical ventilation is known to cause acute lung injury because of the overstretching to alveoli during the treatment of acute respiratory distress syndrome [21,22]. Interestingly, the motility of *Trichoplax adhaerens*, a highly dynamic simple organism, can lead to the fracture of its epithelial tissue [23]. Moreover, cracks may appear around the location of weak adhesion between neighboring cells in confluent epithelial sheets, causing woundlike holes [24] and even fracture failure [25]. Similarly, monolayers can release the excessive hydraulic pressure through the breakage of cell-cell adhesion [26,27]. Although the mechanics of epithelial monolayers is an essential part of its functions, little is known about how fracture failure occurs in response to mechanical stress and large deformation, and a simple theoretical model to characterize monolayer fracture is still lacking.

First, we treat each cell as an individual polygon containing several vertices [Figs. 1(c) and 1(d)] based on the two-dimensional vertex model [28–33]. For simplicity, here we assume the properties of each cell are identical. The energy of the system is

$$U = \sum_{I:\text{cell}} \frac{1}{2} K (A_I - A_0)^2 + \sum_{I:\text{cell}} \frac{1}{2} \Gamma L_I^2 + \sum_{ab:\text{edge}} \Lambda l_{ab}. \quad (1)$$

The first term in Eq. (1) is the energy of cell area elasticity with areal stiffness K [29,34], where A_I and A_0 are the current and preferred area of the Ith cell. The second term represents the perimeter elasticity originating from actomyosin contractility, where Γ is the contractile modulus [35].

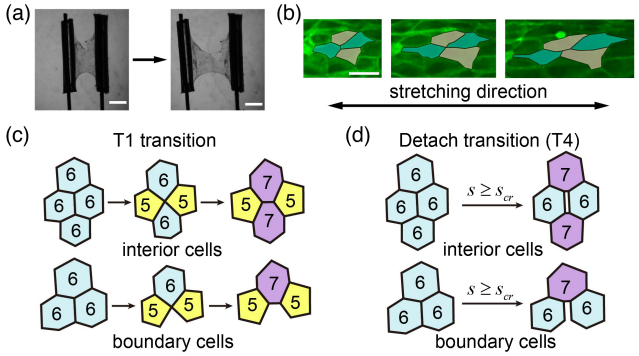

FIG. 1. Topological transitions in cell monolayers. (a) The fracture failure (scale bar, 1 mm) and (b) $T1$ transition under uniaxial tensile loading in experiments (scale bar: 25 μm). See Supplemental Material [37] for details. (c) $T1$ transition in vertex model. (d) Detach transition ($T4$ transition) we defined.

The third term is the interfacial energy with a line tension Λ, which originates from the competition between cortical tension and intercellular adhesion [29,36]. Λ can be negative if adhesion energy is bigger than cortical tension or positive if cortical tension dominates. L_I denotes the perimeter of the Ith cell and l_{ab} is the length of the contact edge connected by adjacent vertices a and b. The morphological changes of the monolayer can be described by $d\mathbf{r}_a/dt = \mathbf{F}_a/\eta$, where η is the viscous coefficient, $\mathbf{r}_a$ and $\mathbf{F}_a = -\partial U/\partial \mathbf{r}_a$ are the coordinates and force acting on vertex a, respectively.

The topological transitions in the classical vertex model are based on geometrical criterions, such as length ($T1$ transition, to model cell intercalation [49]), area ($T2$ transition, to describe cell death [50]), and distance ($T3$ transition, to model cell merging process [44]). For example, when the edge between two neighboring cells is shorter than a threshold, the edge will shrink to a point and another two cells become new neighbors, so that $T1$ transition occurs (see Fig. 1). However, the above geometrical criteria are not relevant to fracture and cannot be used to describe monolayer fracture since they do not allow for the creation of intracellular spacing. To solve this problem, we propose a failure criterion and define a detach transition ($T4$ transition) [Fig. 1(d)], based on the calculation of intercellular stress on each edge (Supplemental Material [37] and Fig. S1). The 2D normal stress on an edge is

$$s_{ab} = F^n_{ab}/l_{ab}, \tag{2}$$

where l_{ab} is edge length, and F^n_{ab} is the normal component of the traction force on this edge. The cell-cell adhesion will break when $s_{ab} > s_{\mathrm{cr}}$, where s_{cr} is the critical stress as a material property of cell-cell contact (e.g., the adhesive links including E-cadherin [51] and tricellular junction proteins [45]). After this detach transition occurs, a crack between two cells appears, and new short edges are created in some cells so that the edge number of these cells increases [Fig. 1(d)]. Similar failure criteria has been used in the system of soft sticky balls connected by springs [23], and nonconfluent epithelium can also be obtained through replacing the original vertex by a small triangular extracellular space in a vertexlike model [46] or through energy minimization in a simple four-cell model [52].

We can normalize all the equations with characteristic length $\sqrt{A_0}$ and characteristic time η/KA_0 and obtain three dimensionless parameters: $\tilde{\Gamma} = \Gamma/KA_0$, $\tilde{\Lambda} = \Lambda/KA_0^{3/2}$, and $\tilde{s}_{\mathrm{cr}} = s_{\mathrm{cr}}/KA_0$. Thus, we have

$$\tilde{U} = \sum_{I:\mathrm{cell}} \frac{1}{2}(\tilde{A}_I - 1)^2 + \sum_{I:\mathrm{cell}} \frac{1}{2}\tilde{\Gamma}\tilde{L}_I^2 + \sum_{ab:\mathrm{edge}} \tilde{\Lambda}\tilde{l}_{ab}. \tag{3}$$

The intracellular stress $\tilde{\sigma}^{\mathrm{cell}}_{xx}$ and tissue stress $\tilde{\sigma}^{\mathrm{tissue}}_{xx}$ can be derived (Supplemental Material [37]).

Now, we can investigate the uniaxial stretching of cell monolayers. If the loading is very quick, there is not enough time for cell rearrangement, which is the case in most experiments [25,26]. In contrast, here we consider a quasistatic displacement-controlled uniaxial tensile test, where the loading is slow enough to allow the system to reach the equilibrium at each loading step and allow cell rearrangement to happen, but fast enough to eliminate the influence of cell division and death. Notice that epithelial cells usually take more than 10 h to finish cell cycle [53], while a typical $T1$ transition occurs in tens of minutes [54]. Therefore, here we neglect cell division and death and only consider $T1$ transition and detachment transition (Fig. 1).

Confluent cell monolayer can undergo a solid-to-liquid transition (SLT) at $\tilde{\Lambda} = -4\tilde{\Gamma}\sqrt{n\tan(\pi/n)}$ [30], where n is the number of cell sides (Fig. S2 [37]). Here, we focus on the solid phase (jammed monolayers) and first consider a hexagonal lattice (Figs. 2 and 3), which is known as the ground state of the solid phase [30,55]. Although hexagonal lattice sounds ideal, it is quite common in tissues, such as marginal cells of stria vascularis [56], *Drosophila* wing disk [57], and lens fiber cells [58]. Here we perform the uniaxial tensile test in the zigzag direction of hexagonal

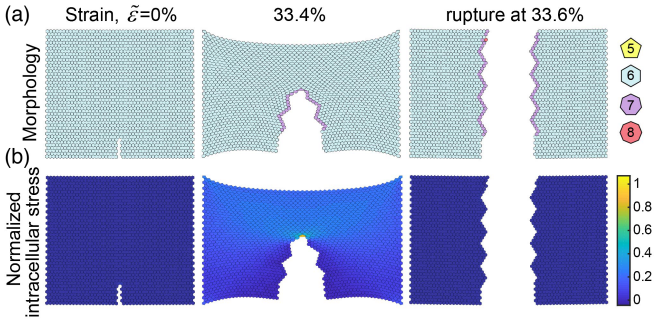

FIG. 2. A brittle monolayer ($\tilde{\Gamma} = 0.16$, $\tilde{\Lambda} = -0.7$, and $\tilde{s}_{\mathrm{cr}} = 3$) under displacement-controlled uniaxial tensile loading. (a) Time evolution of monolayer morphology. (b) Corresponding time evolution of intracellular stress $\tilde{\sigma}^{\mathrm{cell}}_{xx}$. To induce failure in the middle, a nick is made to concentrate stress [25].

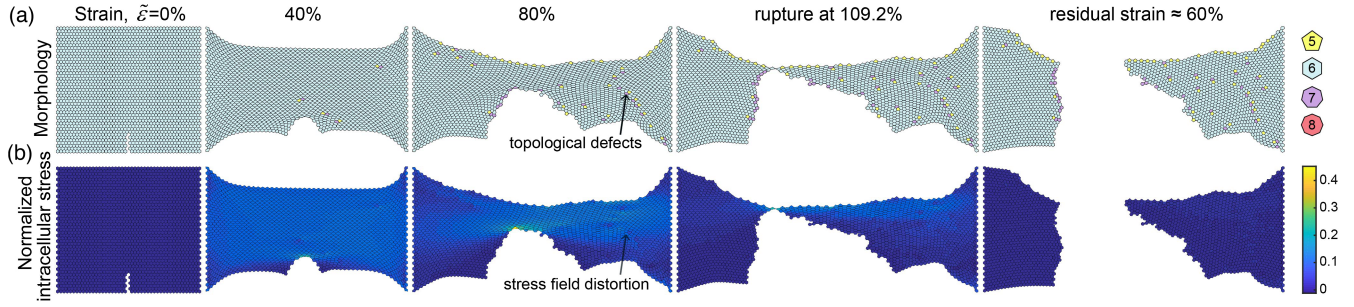

FIG. 3. A ductile monolayer ($\tilde{\Gamma} = 0.16$, $\tilde{\Lambda} = -1.19$, and $\tilde{s}_{cr} = 3$) under displacement-controlled uniaxial tensile loading. (a) Time evolution of monolayer morphology. The plastic deformation is induced by the nucleation and propagation of pentagon-heptagon defects, which are usually seen in graphene. (b) Corresponding time evolution of intracellular stress $\tilde{\sigma}_{xx}^{\text{cell}}$ shows obvious distortions of stress field around pentagon-heptagon defects.

lattice [59]. Interestingly, we find different parameters in this solid region can yield completely different mechanical responses.

Figure 2 and Videos S1 and S2 (in the Supplemental Material [37]) show a clearly catastrophic brittlelike failure without observable plastic elongation, which is further demonstrated by the sharp fracture surface, negligible cell rearrangement [Fig. 4(b)], and plastic strain [Fig. 4(c)]. The corresponding stress-strain curve further confirms its brittlelike nature, in which the sudden fracture occurs at a large elastic strain of 33.4% [blue curve in Fig. 4(a)]. Depending on parameters, the breaking elongation of brittle monolayers can vary greatly from 30% to more than 100% (Fig. S8). In fact, due to their soft nature, a good indicator of brittleness and ductility of soft materials (e.g., tissues and hydrogels) is not the elongation at break, but the plastic deformation before rupture.

Strikingly, as $\tilde{\Lambda}$ decreases to -1.19 in Fig. 3 and Videos S3 and S4 [37], apparent plastic elongation with classical characteristics of ductile fracture are observed. Monolayer rupture occurs at a large strain of 109% with a permanent plastic elongation of 60%. Notably, an apparent necking and rough fracture surfaces are also observed, suggesting significant plastic flow occurs before fracture [Figs. S4(a), S4(b), and S4(d) [37]]. This is further confirmed by its stress-strain relationship [the green curve in Fig. 4(a)].

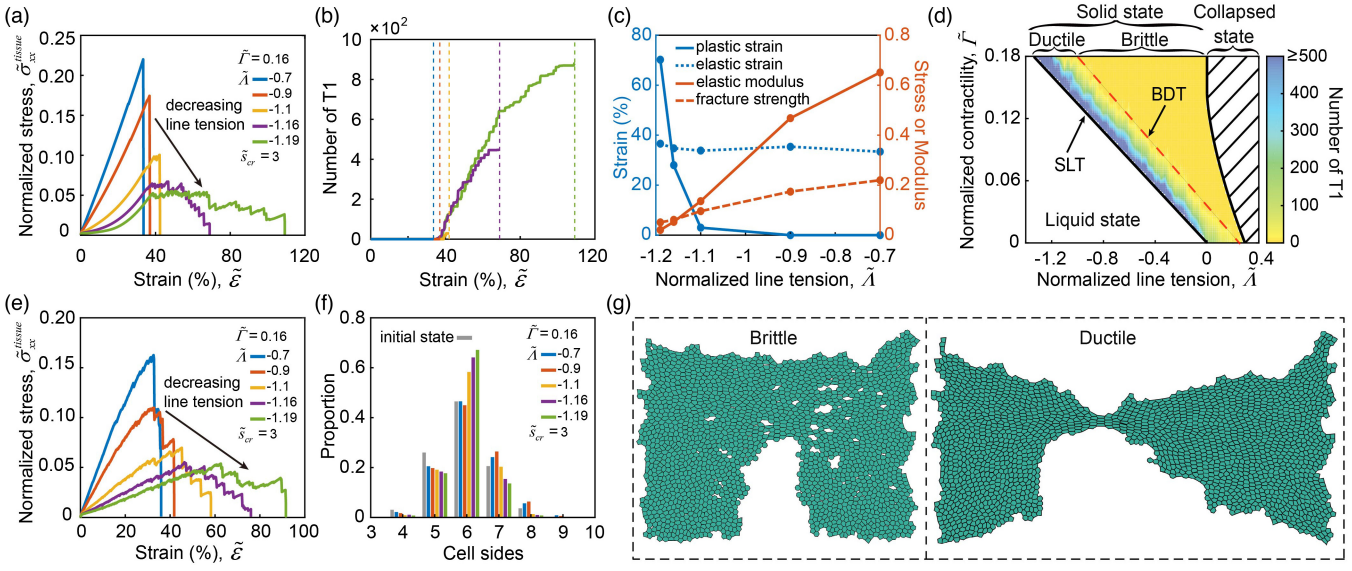

FIG. 4. Brittle-to-ductile transition (BDT) of the epithelial monolayer is controlled by the mechanical properties of single cells and cell-cell contacts. (a)–(d) Hexagonal cell lattice. (a) Stress-strain relationship for various $\tilde{\Lambda}$. (b) The accumulated number of $T1$ transitions during stretching. Dashed lines indicate where curves stop. (c) The elastic strain, plastic strain, elastic modulus, and fracture strength as the function of $\tilde{\Lambda}$. (d) Phase diagram of BDT. (e)–(g) Irregular monolayers. (e) Stress-strain relationship for various $\tilde{\Lambda}$. (f) The proportion of cells with n cell sides before loading begins and after monolayer rupture occurs. (g) Irregular monolayer morphology during brittle and ductile fracture. Left, a brittle case at 35% strain [blue curve in (e)]. Right, a ductile case at 90% strain [green curve in (e)].

Therefore, Figs. 2 and 3 together reveal a clear brittle-to-ductile transition as $\tilde{\Lambda}$ decreases, which is also confirmed by the stress-strain curves in Fig. 4(a).

The plastic deformation in Fig. 3 is very similar to the germ-band elongation during *Drosophila* morphogenesis [47,48]. This plastic deformation results from $T1$ transition, which is also known as cell rearrangement or cell intercalation [17,60–62] as shown in Fig. 1. We find if $T1$ transition occurs inside the monolayer, two pair of pentagon-heptagon defects will appear [Fig. 1(c)]. In contrast, if $T1$ transition occurs on the boundary, only one pair of pentagon-heptagon defects and one pentagonal cell will appear [Fig. 1(c)]. Similar to many 2D materials, e.g., graphene [63], a pentagon-heptagon defect resembles a disclination dipole, which can be regarded as an edge dislocation. We find dislocations keep nucleating on the boundaries, especially near the crack tip, and then propagate to the interior of the cell monolayer and finally end up at another boundary (Fig. 3, Videos S3 and S4, and Fig. S5 [37]). The number of $T1$ transitions increase as the stretching continues [Fig. 4(b)], indicating permanent plastic deformation is accumulating. Thus, we conclude that the external loadings can activate cell rearrangement in ductile cell monolayers.

We also find, besides the stress concentration at the crack tip, that there are obvious distortions of stress field around each pentagon-heptagon defect [Fig. 3(b)], which is quite similar to the theoretical description of a disclination dipole in graphene [63]. Furthermore, as the monolayer becomes more ductile, it will also become softer (indicated by elastic modulus) and more fragile (indicated by fracture strength), yet the elastic range is approximately the same (indicated by maximum elastic strain) as shown in Fig. 3(c).

Similar to the effects of $\tilde{\Lambda}$ [Fig. 4(a)], as $\tilde{\Gamma}$ decreases, there also exists a brittle-to-ductile transition (Fig. S6 [37]). Furthermore, we find that the closer to the solid-fluid transition curve [Fig. 4(d)], i.e., the lower $\tilde{\Lambda}$ and $\tilde{\Gamma}$ [29,30], the more ductile the cell monolayer becomes, indicated by the increase of the cumulative number of $T1$ transitions [Figs. 4(b), 4(d), S6, and S7]. Therefore, we conclude that the brittle-to-ductile transition of the epithelial monolayer is controlled by the mechanical properties of single cells and cell-cell contacts, such as the relative contractile modulus ($\tilde{\Gamma}$), relative line tension ($\tilde{\Lambda}$), and relative intercellular strength ($\tilde{s}_{\mathrm{cr}}$).

Given that in many tissues the cell monolayer is not a regular hexagonal lattice [54,60,64], we also investigate the uniaxial stretching of irregular cell monolayers. The irregular lattice with a diverse number of cell sides is generated through Voronoi tessellation and undergoes a local minimization of free energy, i.e., the annealing process, before stretching. The irregular lattice we obtained through this method [the gray column in Fig. 4(f)] is quite similar to the experimental samples where hexagonal cells are about 40% [64].

We find that the brittle-to-ductile transition also exists in the irregular cell monolayer [Fig. 4(e), Videos S5 and S6 [37]), and its mechanical responses are qualitatively the same as the hexagonal cell monolayer (Figs. S6 and S7). However, since the irregular cell monolayers have more preexisting disclination- and dislocationlike defects compared to the regular hexagonal monolayer, cell rearrangements occur more easily, more frequently, and earlier [55], so that the yield stress and fracture strength of the cell monolayer are smaller. Furthermore, the nonuniform nature of irregular lattice leads to local stress concentration, so that many detachment transitions occur and many small cracks are created during stretching, especially in brittle monolayers [Fig. 4(g), left]. Eventually, these small cracks may coalesce to form woundlike holes, which is in good agreement with the crack morphology observed in experiments [24,25].

Interestingly, in ductile cell monolayers, the irregular lattice becomes more regular, i.e., the proportion of hexagonal cells increases [Fig. 4(f), Video S7 [37]] under uniaxial tensile loading, which is consistent with the prominent increase of topological order of tissues during development [54,57,60,65]. This hexagonal ordering becomes inapparent as the monolayer becomes more brittle, since there is negligible cell rearrangement in brittle monolayers [Fig. 4(f)]. Therefore, these results indicate that the brittle-to-ductile transition can also affect the evolution of topological order of epithelial tissues during development.

To get more insight into brittle-to-ductile transition, we investigate $T1$ transition and detachment transition by using a simple four-cell model [36,66]. Without external force ($\tilde{F} = 0$), the total energy of the four-cell system has two local minimums, i.e., two equilibrium states before and after $T1$ transition, as the length of shared edge changes [Fig. 5(a)]. We find, in this case, the energy barrier for $T1$ transition $\Delta\tilde{U}_0$ becomes smaller as the parameters approach the solid-to-liquid transition boundary [Fig. S10(a) [37]], which is consistent with previous studies [36,66]. When a tensile force $\tilde{F}$ is applied along the zigzag direction, the total energy becomes higher, yet the energy barrier $\Delta\tilde{U}_{\tilde{F}}$ and the equilibrium length of the shared edge before $T1$ transition $\tilde{l}_{\tilde{F}}$ decreases, so that $T1$ transition will happen more easily [Figs. 5(a), 5(b), and S10(b)].

On the other hand, as the external force $\tilde{F}$ increases, the stress along the shared edge $\tilde{s}_{ab}$ will become larger due to the decrease of the equilibrium length of the shared edge [see Eq. (2)] so that the detachment transition is also more likely to occur. Thus, $T1$ transition and detachment transition compete with each other to determine which process will happen first. We find $T1$ transition will occur first for small $\tilde{\Lambda}$ or $\tilde{\Gamma}$, while detachment transition will occur first for large $\tilde{\Lambda}$ or $\tilde{\Gamma}$ [Figs. 5(c) and S11(b) [37]] during the loading process. Further calculation shows that $T1$ transition will occur first near the boundary of solid-to-liquid transition in the phase diagram, so that the cell monolayer is ductile [Fig. 5(d)], which well explains the

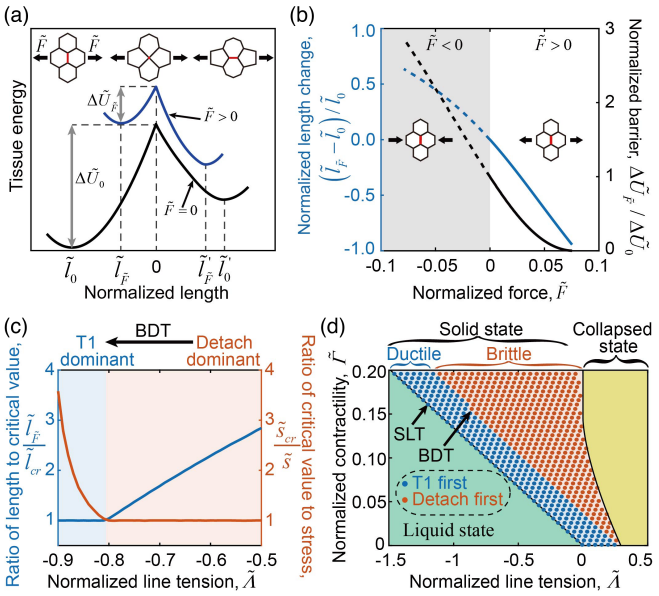

FIG. 5. Competition between $T1$ and detach transition leads to the observed brittle-to-ductile transition. (a) Energy landscape with or without external force $\tilde{F}$ on the left and right boundaries, showing energy barrier and equilibrium length of shared edge (red line) before and after $T1$ transition ($\tilde{\Gamma} = 0.12$, $\tilde{\Lambda} = -0.6$). (b) Normalized energy barrier $\Delta\tilde{U}_{\tilde{F}}/\Delta\tilde{U}_0$ and normalized equilibrium length of shared edge $(\tilde{l}_{\tilde{F}} - \tilde{l}_0)/\tilde{l}_0$ change with $\tilde{F}$. (c) Competition between $T1$ and detachment transition under tensile loading ($\tilde{\Gamma} = 0.12$, $\tilde{s}_{\rm cr} = 2$). (d) Phase diagram of four-cell system under stretching ($\tilde{s}_{\rm cr} = 5$).

brittle-to-ductile transition we found in Fig. 4. We further demonstrate that the boundary of brittle-to-ductile transition is mainly determined by $\tilde{s}_{\rm cr}$, and the decrease of $\tilde{s}_{\rm cr}$ leads to a larger brittle region in the phase diagram [Fig. S11(c)], which is similar to the effect of ethylenediamine tetra-acetic acid, a chelating agent that disrupts the adhesive links at the cell-cell interface and causes the monolayer to be more fragile [25]. Therefore, we conclude that the competition between $T1$ transition and detachment transition leads to the observed brittle-to-ductile transition of the cell monolayer.

In summary, we define a new type of topological transition, i.e., detach transition or $T4$ transition, so that the fracture failure can be studied in the framework of a vertex model. We show that there exists a brittle-to-ductile transition in epithelial monolayers when the mechanical properties of individual cells and cell-cell contacts change, and the transition is attributed to the competition between cell rearrangement and cell detachment. Interestingly, in ductile monolayers, cell intercalation can lead to the plastic deformation characterized by the nucleation and propagation of pentagon-heptagon defects that are commonly seen in 2D materials. Our results demonstrate how the mechanical properties of individual living cells and their interaction determine the mechanical response of larger scale tissues. The brittle-to-ductile transition still exists even when the healing process is present (Fig. S9 [37]). Similar brittle-to-ductile transitions were also observed in amorphous solids when attraction (similar to the line tension in our work) [67] and annealing degree changed [68,69]. Our findings provide a new theoretical framework to study the mechanics of cell monolayers and may also have important implications for other relevant biological processes accompanied by significant cell rearrangement and detachment.

This work was supported by the National Natural Science Foundation of China (Grants No. 12025207 and No. 11872357), the Fundamental Research Funds for the Central Universities, the Strategic Priority Research Program of the Chinese Academy of Sciences (Grant No. XDB22040403). This work was partially carried out at the University of Science and Technology of China Center for Micro and Nanoscale Research and Fabrication.

*Corresponding author.
jianghy@ustc.edu.cn

[1] M. Aliee, J.-C. Röper, K. P. Landsberg, C. Pentzold, T. J. Widmann, F. Jülicher, and C. Dahmann, Physical mechanisms shaping the *Drosophila* dorsoventral compartment boundary, Curr. Biol. **22**, 967 (2012).
[2] M. Rauzi, P. Verant, T. Lecuit, and P.-F. Lenne, Nature and anisotropy of cortical forces orienting *Drosophila* tissue morphogenesis, Nat. Cell Biol. **10**, 1401 (2008).
[3] L. Pasakarnis, E. Frei, E. Caussinus, M. Affolter, and D. Brunner, Amnioserosa cell constriction but not epidermal actin cable tension autonomously drives dorsal closure, Nat. Cell Biol. **18**, 1161 (2016).
[4] C. R. Ethier and C. A. Simmons, *Introductory Biomechanics: From Cells to Organisms* (Cambridge University Press, Cambridge, England, 2007).
[5] Y.-c. Fung, *Biomechanics: Mechanical Properties of Living Tissues* (Springer Science & Business Media, New York, 2013).
[6] P. Cai, B. Hu, W. R. Leow, X. Wang, X. J. Loh, Y. Wu, and X. Chen, Biomechano-interactive materials and interfaces, Adv. Mater. **30**, 1800572 (2018).
[7] R. Maiti, L.-C. Gerhardt, Z. S. Lee, R. A. Byers, D. Woods, J. A. Sanz-Herrera, S. E. Franklin, R. Lewis, S. J. Matcher, and M. J. Carré, *In vivo* measurement of skin surface strain and sub-surface layer deformation induced by natural tissue stretching, J. Mech. Behav. Biomed. Mater. **62**, 556 (2016).
[8] J. Ando and K. Yamamoto, Effects of shear stress and stretch on endothelial function, Antioxid. Redox Signal. **15**, 1389 (2011).
[9] Z. He, J. Ritchie, J. S. Grashow, M. S. Sacks, and A. P. Yoganathan, *In vitro* dynamic strain behavior of the mitral valve posterior leaflet, J. Biomech. Eng. **127**, 504 (2005).
[10] M. S. Sacks, Y. Enomoto, J. R. Graybill, W. D. Merryman, A. Zeeshan, A. P. Yoganathan, R. J. Levy, R. C. Gorman, and J. H. Gorman, *In-vivo* dynamic deformation of the mitral valve anterior leaflet, Ann. Thorac. Surg. **82**, 1369 (2006).

[11] T. P. Wyatt, J. Fouchard, A. Lisica, N. Khalilgharibi, B. Baum, P. Recho, A. J. Kabla, and G. T. Charras, Actomyosin controls planarity and folding of epithelia in response to compression, Nat. Mater. **19**, 109 (2020).
[12] T. Tallinen, J. Y. Chung, F. Rousseau, N. Girard, J. Lefvre, and L. Mahadevan, On the growth and form of cortical convolutions, Nat. Phys. **12**, 588 (2016).
[13] B. D. Simons, Getting your gut into shape, Science **342**, 203 (2013).
[14] J. Sidhaye and C. Norden, Concerted action of neuroepithelial basal shrinkage and active epithelial migration ensures efficient optic cup morphogenesis, eLife **6**, e22689 (2017).
[15] C. Guillot and T. Lecuit, Mechanics of epithelial tissue homeostasis and morphogenesis, Science **340**, 1185 (2013).
[16] T. P. Wyatt, A. R. Harris, M. Lam, Q. Cheng, J. Bellis, A. Dimitracopoulos, A. J. Kabla, G. T. Charras, and B. Baum, Emergence of homeostatic epithelial packing and stress dissipation through divisions oriented along the long cell axis, Proc. Natl. Acad. Sci. U.S.A. **112**, 5726 (2015).
[17] C. Bertet, L. Sulak, and T. Lecuit, Myosin-dependent junction remodelling controls planar cell intercalation and axis elongation, Nature (London) **429**, 667 (2004).
[18] S. A. Gudipaty, J. Lindblom, P. D. Loftus, M. J. Redd, K. Edes, C. Davey, V. Krishnegowda, and J. Rosenblatt, Mechanical stretch triggers rapid epithelial cell division through piezo1, Nature (London) **543**, 118 (2017).
[19] G. T. Eisenhoffer, P. D. Loftus, M. Yoshigi, H. Otsuna, C.-B. Chien, P. A. Morcos, and J. Rosenblatt, Crowding induces live cell extrusion to maintain homeostatic cell numbers in epithelia, Nature (London) **484**, 546 (2012).
[20] V. W. Tang and W. M. Brieher, FSGS3/CD2AP is a barbed-end capping protein that stabilizes actin and strengthens adherens junctions, J. Cell Biol. **203**, 815 (2013).
[21] G. Matute-Bello, C. W. Frevert, and T. R. Martin, Animal models of acute lung injury, Am. J. Physiol. Lung Cell Mol. Physiol. **295**, L379 (2008).
[22] N. E. Vlahakis and R. D. Hubmayr, Cellular stress failure in ventilator-injured lungs, Am. J. Respir. Crit. Care Med. **171**, 1328 (2005).
[23] V. N. Prakash, M. S. Bull, and M. Prakash, Motility-induced fracture reveals a ductile-to-brittle crossover in a simple animals epithelia, Nat. Phys. **17**, 504 (2021).
[24] S. R. K. Vedula, H. Hirata, M. H. Nai, A. Brugues, Y. Toyama, X. Trepat, C. T. Lim, and B. Ladoux, Epithelial bridges maintain tissue integrity during collective cell migration, Nat. Mater. **13**, 87 (2014).
[25] A. R. Harris, L. Peter, J. Bellis, B. Baum, A. J. Kabla, and G. T. Charras, Characterizing the mechanics of cultured cell monolayers, Proc. Natl. Acad. Sci. U.S.A. **109**, 16449 (2012).
[26] L. Casares, R. Vincent, D. Zalvidea, N. Campillo, D. Navajas, M. Arroyo, and X. Trepat, Hydraulic fracture during epithelial stretching, Nat. Mater. **14**, 343 (2015).
[27] E. Latorre, S. Kale, L. Casares, M. Gmez-Gonzlez, M. Uroz, L. Valon, R. V. Nair, E. Garreta, N. Montserrat, A. Del Campo *et al.*, Active superelasticity in three-dimensional epithelia of controlled shape, Nature (London) **563**, 203 (2018).
[28] T. Nagai and H. Honda, A dynamic cell model for the formation of epithelial tissues, Philos. Mag. B **81**, 699 (2001).
[29] R. Farhadifar, J.-C. Röper, B. Aigouy, S. Eaton, and F. Jülicher, The influence of cell mechanics, cell-cell interactions, and proliferation on epithelial packing, Curr. Biol. **17**, 2095 (2007).
[30] D. B. Staple, R. Farhadifar, J.-C. Röper, B. Aigouy, S. Eaton, and F. Jülicher, Mechanics and remodelling of cell packings in epithelia, Eur. Phys. J. E **33**, 117 (2010).
[31] A. G. Fletcher, M. Osterfield, R. E. Baker, and S. Y. Shvartsman, Vertex models of epithelial morphogenesis, Biophys. J. **106**, 2291 (2014).
[32] S. Lin, B. Li, G. Lan, and X. Feng, Activation and synchronization of the oscillatory morphodynamics in multicellular monolayer, Proc. Natl. Acad. Sci. U.S.A. **114**, 8157 (2017).
[33] G.-K. Xu, Y. Liu, and B. Li, How do changes at the cell level affect the mechanical properties of epithelial monolayers?, Soft Matter **11**, 8782 (2015).
[34] A. Merzouki, O. Malaspinas, A. Trushko, A. Roux, and B. Chopard, Influence of cell mechanics and proliferation on the buckling of simulated tissues using a vertex model, Nat. Comput. **17**, 511 (2018).
[35] S. Lin, S. Ye, G. Xu, B. Li, and X. Feng, Dynamic migration modes of collective cells, Biophys. J. **115**, 1826 (2018).
[36] D. Bi, J. Lopez, J. M. Schwarz, and M. L. Manning, A density-independent rigidity transition in biological tissues, Nat. Phys. **11**, 1074 (2015).
[37] See Supplemental Material at http://link.aps.org/supplemental/10.1103/PhysRevLett.128.018101 for more methods, discussions, figures, and video files, which includes Refs. [15,23,25,29,30,36,38–48].
[38] S. Ishihara and K. Sugimura, Bayesian inference of force dynamics during morphogenesis, J. Theor. Biol. **313**, 201 (2012).
[39] X. Yang, D. Bi, M. Czajkowski, M. Merkel, M. L. Manning, and M. C. Marchetti, Correlating cell shape and cellular stress in motile confluent tissues. Proc. Natl. Acad. Sci. U.S.A. **114**, 12663 (2017).
[40] A. Nestor-Bergmann, G. Goddard, S. Woolner, and O. E. Jensen, Relating cell shape and mechanical stress in a spatially disordered epithelium using a vertex-based model, Math. Med. Biol. **35**, i1 (2018).
[41] G. Charras and A. S. Yap, Tensile forces and mechanotransduction at cell-cell junctions, Curr. Biol. **28**, R445 (2018).
[42] K. K. Chiou, L. Hufnagel, and B. I. Shraiman, Mechanical stress inference for two dimensional cell arrays, PLoS Comput. Biol. **8**, e1002512 (2012).
[43] A. G. Fletcher, J. M. Osborne, P. K. Maini, and D. J. Gavaghan, Implementing vertex dynamics models of cell populations in biology within a consistent computational framework, Prog. Biophys. Molec. Biol. **113**, 299 (2013).
[44] T. Nagai and H. Honda, Computer simulation of wound closure in epithelial tissues: Cell-basal-lamina adhesion, Phys. Rev. E **80**, 061903 (2009).
[45] S. Byri, T. Misra, Z. A. Syed, T. Bätz, J. Shah, L. Boril, J. Glashauser, T. Aegerter-Wilmsen, T. Matzat, B. Moussian *et al.*, The triple-repeat protein anakonda controls epithelial

tricellular junction formation in *Drosophila*, Dev. Cell **33**, 535 (2015).
[46] S. Kim, M. Pochitaloff, G. A. Stooke-Vaughan, and O. Campàs, Embryonic tissues as active foams, Nat. Phys. **17**, 859 (2021).
[47] C. Collinet, M. Rauzi, P.-F. Lenne, and T. Lecuit, Local and tissue-scale forces drive oriented junction growth during tissue extension, Nat. Cell Biol. **17**, 1247 (2015).
[48] J. A. Zallen and E. Wieschaus, Patterned gene expression directs bipolar planar polarity in *Drosophila*, Dev. Cell **6**, 343 (2004).
[49] D. Weaire and N. Rivier, Soap, cells and statistics–random patterns in two dimensions, Contemp. Phys. **25**, 59 (1984).
[50] T. Nagai, H. Honda, and M. Takemura, Simulation of cell patterning triggered by cell death and differential adhesion in *Drosophila* wing, Biophys. J. **114**, 958 (2018).
[51] T. Lecuit and A. S. Yap, E-cadherin junctions as active mechanical integrators in tissue dynamics, Nat. Cell Biol. **17**, 533 (2015).
[52] N. I. Petridou, B. Corominas-Murtra, C. P. Heisenberg, and E. Hannezo, Rigidity percolation uncovers a structural basis for embryonic tissue phase transitions, Cell **184**, 1914 (2021).
[53] B. Alberts, D. Bray, K. Hopkin, A. Johnson, J. Lewis, M. Raff, K. Roberts, and P. Walter, *Essential Cell Biology* (Garland, New York, 1998).
[54] S. Curran, C. Strandkvist, J. Bathmann, M. de Gennes, A. Kabla, G. Salbreux, and B. Baum, Myosin II controls junction fluctuations to guide epithelial tissue ordering, Dev. Cell **43**, 480 (2017).
[55] S. Kim, Y. Wang, and S. Hilgenfeldt, Universal Features of Metastable State Energies in Cellular Matter, Phys. Rev. Lett. **120**, 248001 (2018).
[56] M. Anniko, Surface structure of stria vascularis in the guinea pig cochlea normal morphology and atoxyl-induced pathologic changes, Acta Otolaryngol. **82**, 343 (1976).
[57] A.-K. Classen, K. I. Anderson, E. Marois, and S. Eaton, Hexagonal packing of *Drosophila* wing epithelial cells by the planar cell polarity pathway, Dev. Cell **9**, 805 (2005).
[58] M. A. Cooper, A. I. Son, D. Komlos, Y. Sun, N. J. Kleiman, and R. Zhou, Loss of ephrin-a5 function disrupts lens fiber cell packing and leads to cataract, Proc. Natl. Acad. Sci. U.S.A. **105**, 16620 (2008).
[59] H. Zhao, K. Min, and N. R. Aluru, Size and chirality dependent elastic properties of graphene nanoribbons under uniaxial tension, Nano Lett. **9**, 3012 (2009).
[60] D.-Y. Chen, J. Crest, S. J. Streichan, and D. Bilder, Extracellular matrix stiffness cues junctional remodeling for 3D tissue elongation, Nat. Commun. **10**, 3339 (2019).
[61] M. F. Staddon, K. E. Cavanaugh, E. Munro, M. L. Gardel, and S. Banerjee, Mechanosensitive junction remodeling promotes robust epithelial morphogenesis, Biophys. J. **117**, 1739 (2019).
[62] A. Vichas and J. A. Zallen, Translating cell polarity into tissue elongation, Semin. Cell Dev. Biol. **22**, 858 (2011).
[63] Y. Wei, J. Wu, H. Yin, X. Shi, R. Yang, and M. Dresselhaus, The nature of strength enhancement and weakening by pentagon-heptagon defects in graphene, Nat. Mater. **11**, 759 (2012).
[64] M. C. Gibson, A. B. Patel, R. Nagpal, and N. Perrimon, The emergence of geometric order in proliferating metazoan epithelia, Nature (London) **442**, 1038 (2006).
[65] K. Sugimura and S. Ishihara, The mechanical anisotropy in a tissue promotes ordering in hexagonal cell packing, Development **140**, 4091 (2013).
[66] D. Bi, J. H. Lopez, J. M. Schwarz, and M. L. Manning, Energy barriers and cell migration in densely packed tissues, Soft Matter **10**, 1885 (2014).
[67] O. Dauchot, S. Karmakar, I. Procaccia, and J. Zylberg, Athermal brittle-to-ductile transition in amorphous solids, Phys. Rev. E **84**, 046105 (2011).
[68] M. Ozawa, L. Berthier, G. Biroli, A. Rosso, and G. Tarjus, Random critical point separates brittle and ductile yielding transitions in amorphous materials, Proc. Natl. Acad. Sci. U.S.A. **115**, 6656 (2018).
[69] H. J. Barlow, J. O. Cochran, and S. M. Fielding, Ductile and Brittle Yielding in Thermal and Athermal Amorphous Materials, Phys. Rev. Lett. **125**, 168003 (2020).